



# New secondary phosphate mineral occurrences and their crystal chemistry, at the Hagendorf Süd pegmatite, Bavaria

Erich Keck<sup>1</sup>, Ian E. Grey<sup>2</sup>, Colin M. MacRae<sup>2</sup>, Stephanie Boer<sup>3</sup>, Rupert Hochleitner<sup>4</sup>,  
Christian Rewitzer<sup>5</sup>, William G. Mumme<sup>2</sup>, A. Matt Glenn<sup>2</sup>, and Cameron Davidson<sup>2</sup>

<sup>1</sup>Algunderweg 3, 92694 Etzenricht, Germany

<sup>2</sup>Mineral Resources, CSIRO, Private Bag 10, Clayton South, Victoria 3169, Australia

<sup>3</sup>Australian Synchrotron, ANSTO, 800 Blackburn Road, Clayton, Victoria 3168, Australia

<sup>4</sup>Bavarian State Collection for Mineralogy (SNSB), Theresienstrasse 41, 80333 Munich, Germany

<sup>5</sup>Stadtplatz 17, 93437 Furth im Wald, Germany

**Correspondence:** Ian E. Grey (ian.grey@csiro.au)

Received: 5 August 2022 – Revised: 7 September 2022 – Accepted: 12 September 2022 – Published: 10 October 2022

**Abstract.** First occurrences from the Hagendorf Süd pegmatite of the secondary phosphate minerals kenngottite,  $\text{Mn}_3^{2+}\text{Fe}_4^{3+}(\text{PO}_4)_4(\text{OH})_6(\text{H}_2\text{O})_2$ ; allanpringite,  $\text{Fe}_3^{3+}(\text{PO}_4)_2(\text{OH})_3 \cdot 5\text{H}_2\text{O}$ ; iangreyite,  $\text{Ca}_2\text{Al}_7(\text{PO}_4)_2(\text{PO}_3\text{OH})_2(\text{OH},\text{F})_{15} \cdot 8\text{H}_2\text{O}$ ; and nizamoffite,  $\text{MnZn}_2(\text{PO}_4)_2(\text{H}_2\text{O})_4$ , are reported with characterisation of their crystal chemistry and phase associations. A synchrotron single-crystal structure refinement for kenngottite shows that it has the same level of disordering (75%/25%) of  $\text{Fe}^{3+}$  in adjacent octahedra along the 5 Å axis as for type-locality kenngottite from Krásno, Czech Republic. This is explained in terms of 1 : 1 fine-scale mixing of domains of ordered kenngottite-type and souzalite-type structures. Allanpringite occurs in an unusual epitaxial relationship to associated strunzite. The epitaxy is explained by the close metrical and structural match of common planes in the two minerals, (010) for allanpringite and (100) for strunzite. Iangreyite occurs in close association with perhamite in 30 µm spheroids. The characterisation results support a paragenesis of iangreyite from perhamite by selective leaching of silica from the layer structure of perhamite and rejoining of the layers by fusion of  $\text{AlO}_4$  tetrahedra from adjacent layers into  $\text{AlO}_2(\text{OH})_3$  trigonal bipyramids.

## 1 Introduction

The Hagendorf Süd pegmatite is the largest quartz–feldspar body of the Pleystein–Hagendorf pegmatites in the Upper Palatinate (Oberpfalz), in north-eastern Bavaria (49°39′1″ N, 12°27′35″ E). It was mined for its ceramic-grade feldspar from 1894 until 1984 and additionally in the 1950s, for lithium from triphylite,  $\text{Li}(\text{Fe},\text{Mn})\text{PO}_4$ . For the first 30 years, the mine operated as an open-cut mine, but in the 1920s several shafts were sunk, and by the 1950s the mining had descended below 60 m. Rich phosphate mineralisation zones were encountered between the central quartz zone and a sodium-feldspar (cleavelandite) envelope (see Fig. 1 in Birch et al., 2018). These extend from about 60 to 93 m below the surface and contain triphylite, zwieselite, fluorapatite and hagendorfite as the main primary phosphate minerals (Mücke, 1981), together with a host of secondary minerals. During

the mine operation, up to its closure and flooding in 1984, the collection of mineral specimens resulted in large repositories being built up in museum and private collections. To date, 25 new phosphate mineral species have been discovered and approved as new minerals for the locality. A description of type-locality minerals discovered since the mine closure is given by Birch et al. (2018). In addition, Mindat lists another 166 valid phosphate minerals that have been identified from Hagendorf Süd. Detailed studies on the geology and mineralogy of the Pleystein–Hagendorf pegmatites have been reported by Schmid (1955), Forster and Kummer (1974), Strunz et al. (1975), Keck (1983), Mücke (1981), Mücke et al. (1981), and Dill (2015).

During ongoing studies on specimens collected by Erich Keck and Christian Rewitzer, several species not previously reported for the Hagendorf Süd locality have been

identified. They are the recently approved kenngottite,  $\text{Mn}_3^{2+}\text{Fe}_4^{3+}(\text{PO}_4)_4(\text{OH})_6(\text{H}_2\text{O})_2$  (Sejkora et al., 2019); allanpringite,  $\text{Fe}_3^{3+}(\text{PO}_4)_2(\text{OH})_3 \cdot 5\text{H}_2\text{O}$  (Kolitsch et al., 2006); iangreyite,  $\text{Ca}_2\text{Al}_7(\text{PO}_4)_2(\text{PO}_3\text{OH})_2(\text{OH},\text{F})_{15} \cdot 8\text{H}_2\text{O}$  (Mills et al., 2011); and nizamoffite,  $\text{MnZn}_2(\text{PO}_4)_2(\text{H}_2\text{O})_4$  (Kampf et al., 2013). Characterisation data for kenngottite have been published only for a specimen from the type locality, the Stannum mine, Krásno ore district, Czech Republic (Sejkora et al., 2019), although Mindat shows a photo of a kenngottite specimen from the Serra Branca pegmatite, Brazil. The type locality for allanpringite is the dump of the abandoned Grube Mark iron mine, Taunus area, Germany (Kolitsch et al., 2006). Occurrences of allanpringite have recently been described from two localities in the Czech Republic by Vrtiška et al. (2019, 2020). Iangreyite was described by Mills et al. (2011) from co-localities: the Silver Coin mine, Nevada, USA, and the Krásno ore district, Czech Republic. Mindat mentions Norway as the only other country where iangreyite has been identified. The type locality for nizamoffite is the Palermo no. 1 pegmatite, New Hampshire, USA (Kampf et al., 2013). Mindat lists only one other locality, the Foote lithium mine, North Carolina, USA. We report here the crystal-chemical characterisation of occurrences of kenngottite, allanpringite, iangreyite and nizamoffite in specimens collected at the Hagendorf Süd pegmatite.

## 2 Experimental methods

Three of the minerals studied had in common their extremely small crystal dimensions, with thicknesses in the sub-micrometre range. Their microtexture was characterised by back-scattered electron (BSE) imaging using an FEI Quanta 400 environmental scanning electron microscope (ESEM) operated at 15 keV and typically 0.5 nA. The microscope is equipped with a Bruker XFlash Si-drift energy-dispersive X-ray spectrometry (EDS) detector which was used for semiquantitative elemental analyses, identifying minor and trace elements for electron microprobe (EMP) microanalysis, and helping to identify associated minerals. For EMP analyses, specimens were mounted in a polished section, carbon coated and analysed using wavelength-dispersive spectrometry on a JEOL JXA-8500F Hyperprobe operated at an accelerating voltage of 15 kV and a beam current of typically 2 nA. The electron beam was defocused to 5  $\mu\text{m}$ , where crystal size permitted, to minimise beam damage. Standards used were wollastonite (Ca  $K\alpha$ ),  $\text{MnSiO}_3$  (Mn  $K\alpha$ ), hematite (Fe  $K\alpha$ ),  $\text{MgAl}_2\text{O}_4$  (Mg  $K\alpha$ ), phosphophyllite (Zn  $K\alpha$ ) and berlinite (Al and P  $K\alpha$ ).

Powder X-ray diffraction patterns were recorded using a Philips X'Pert MPD (multi-purpose diffractometer) diffractometer with a 3 kW Co tube (Co  $K\alpha$ ), operated at 40 kV and 55 mA. The very small quantities of mineral available required care with grinding in a micro-mortar and dispersion on a silicon disc as a zero-background sample support.

Diffraction patterns were usually recorded from 5 to 70° in  $2\theta$  with a step size of 0.033° and a total data collection time of 2 h. Profile refinements were made using the programme FullProf (Rodríguez-Carvajal, 1990).

A single-crystal (SC) X-ray data collection on kenngottite was made at the microfocus beamline, MX2, of the Australian Synchrotron (Aragao et al., 2018). Data were collected using a DECTRIS EIGER X 16M detector and monochromatic radiation with a wavelength of 0.71073 Å. The crystals were maintained at 100 K in an open-flow nitrogen cryostream during data collections. The diffraction data were collected using a single 36 s sweep of 360° rotation around phi. The resulting dataset consists of 3600 individual images with an approximate phi angle of each image being 0.1°. The raw intensity dataset was processed using XDS (X-ray Detector Software) software to produce data files that were analysed WinGX (Farrugia, 1999) and Jana2006 (Petříček et al., 2014).

## 3 Mineral occurrence and associations

Kenngottite, allanpringite and iangreyite were identified in specimens collected by Erich Keck at the Hagendorf Süd mine in the 1970s and are now in his private collection and in the collections of the Bavarian State Collection for Mineralogy (SNSB). Kenngottite (specimen Hag510) has the museum registration number MSM 38033. All specimens were collected from between the 60 and 87 m levels of the mine, in cavernous regions where extensive alteration (oxidation/hydration) of the primary phosphate minerals had occurred.

Kenngottite, found associated with rockbridgeite paragenesis at the 76 m level of the mine, is commonly present as earthy, fine-grained yellow crusts (Fig. 1a) coating nodules of a rockbridgeite-group mineral or infilling vugs lined with rockbridgeite and hureaulite,  $\text{Mn}_5^{2+}(\text{PO}_3\text{OH})_2(\text{PO}_4)_2 \cdot 4\text{H}_2\text{O}$ . EMP analyses of the associated rockbridgeite gave a composition of  $(\text{Mn}_{0.8}^{2+}\text{Fe}_{0.6}^{2+}\text{Fe}_{0.4}^{3+}\square_{0.2})(\text{Fe}^{3+})_3(\text{PO}_4)_3(\text{OH})_4(\text{H}_2\text{O})$  ( $\square$  = vacancy). Based on the recently approved rockbridgeite-group nomenclature (Grey et al., 2019), this corresponds to a potentially new member of the group “manganrockbridgeite” and would require CNMNC (Commission on New Minerals, Nomenclature and Classification) approval as a new mineral species. The microtexture of the earthy crusts of kenngottite, such as shown in Fig. 1a, is illustrated in Fig. 1b. It comprises an open structure of ultrafine fibres, a few micrometres long and only 0.1–0.2  $\mu\text{m}$  in diameter. At the surface of the crust, some compaction has occurred, but a high microporosity remains, as reflected in very low EMP oxide totals of only 60 wt %–70 wt % compared to 90 % expected for the pure mineral.

Kenngottite also occurs in better crystallised forms. Figure 1c shows sprays and clumps of yellow laths which contain sub-parallel clusters of fine needles in specimen

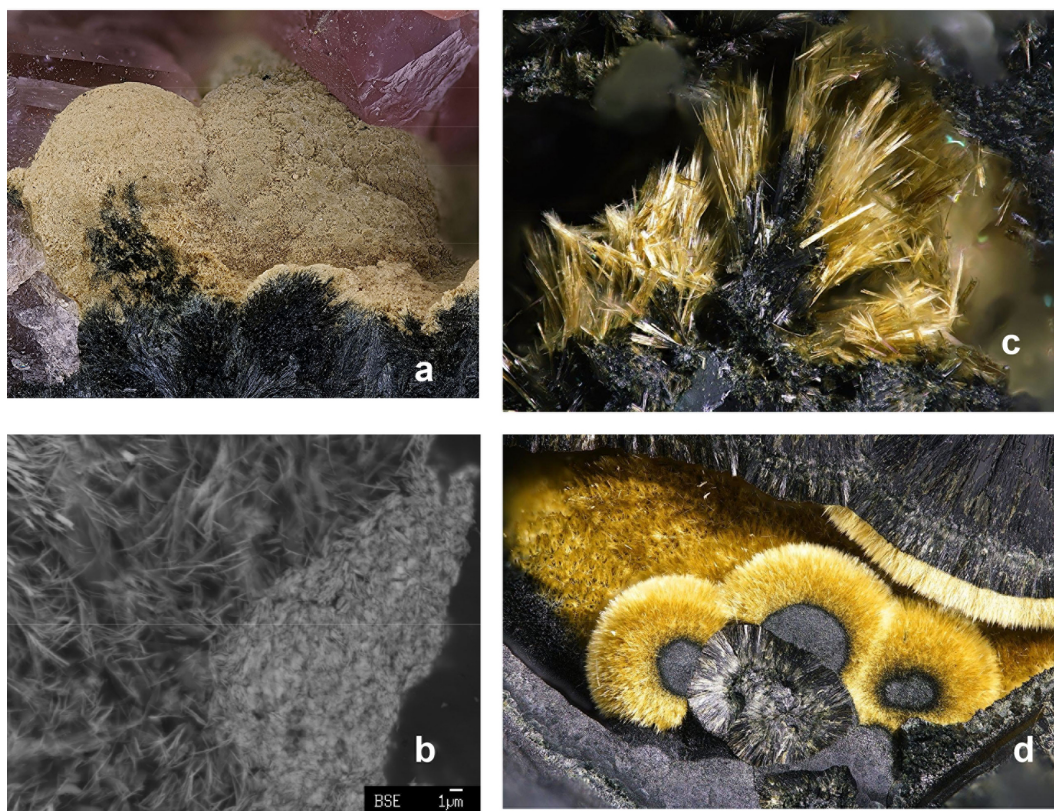


**Figure 1.** (a) Earthy yellow kenngottite crust on rockbridgeite, associated with pink hureaulite in specimen IGC135 (FOV = 4.4 mm; field of view). (b) SEM BSE image showing microtexture of earthy kenngottite. (c) Yellow kenngottite fibres on rockbridgeite in specimen Hag510 (FOV = 1 mm). (d) Radial growth of kenngottite on rockbridgeite (FOV = 3.9 mm). Photo credit: (a) Volker Betz; (c, d) Christian Rewitzer.

Hag510. This specimen consists of black, radiating laths of rockbridgeite intergrown with platelets of hematite. Voids in the rockbridgeite are completely filled with pinkish intergrown crystals of hureaulite up to 5 mm. Open voids with coarse crystallised rockbridgeite and free platelets of hematite show free-standing yellowish to olive-green and olive-brown needles up to 0.1 mm long grown on rockbridgeite and hematite. The kenngottite needles are younger than rockbridgeite and hematite, which constitute the sole direct-contact paragenesis. Other minerals found with the rockbridgeite/hureaulite/kenngottite associations include coriainevite, tavorite, switzerite, bermanite, jahnsite-group minerals, stewartite, laeuite and pseudolaueite. Figure 1d shows radial growth of bright-yellow kenngottite needles on rockbridgeite type. The spheroids in the foreground are ~ 1 mm in diameter.

Allanpringite has so far been found in only one specimen, IGC133. Hemispherical clusters, about 1 mm in diameter (Fig. 2a), of radiating needles with a silvery sheen were located in a corrosion cavity in dark-coloured altered zwieselite. High-magnification SEM images show the allanpringite as epitaxial overgrowths on strunzite (Fig. 2b). Other associated minerals include leucophosphate, cyrilovite, bearaunite, strengite and very well-developed autunite and tor-

bernite. Allanpringite was identified through its PXRD (powder diffraction) pattern and EMP analyses.

Iangreyite occurs as small (~ 30 µm diameter) spheroids clustered not only on light-coloured altered zwieselite but also on residual columbite, FeNb<sub>2</sub>O<sub>6</sub>, as shown in Fig. 3a. An ESEM examination of the spheroids shows a microtexture comprising a honeycomb-like network of intersecting curved laths that are up to 5 µm long but only 0.1–0.2 µm thick (Fig. 3b). A similar microtexture was reported for iangreyite from the Krásno ore district, Czech Republic (Mills et al., 2011). In addition to iangreyite and perhamite, cavities in the altered zwieselite host benyacarite, fluellite, strunzite and jahnsite.

Nizamoffite was identified by Christian Rewitzer in specimens he collected in the late 1970s from near the 60 m level of the mine. Representative specimens are in the Bavarian State Collection for Mineralogy under the museum registration number MSM 38034. Nizamoffite occurs in cavities on dark-green, radiating rockbridgeite. It is associated with bermanite, laeuite, fluorapatite and black manganese oxide masses. A photo of a 2 mm nizamoffite crystal mass is shown in Fig. 4.

According to the paragenetic classification of phosphate minerals at Hagedorf by Mücke (1981), the four minerals

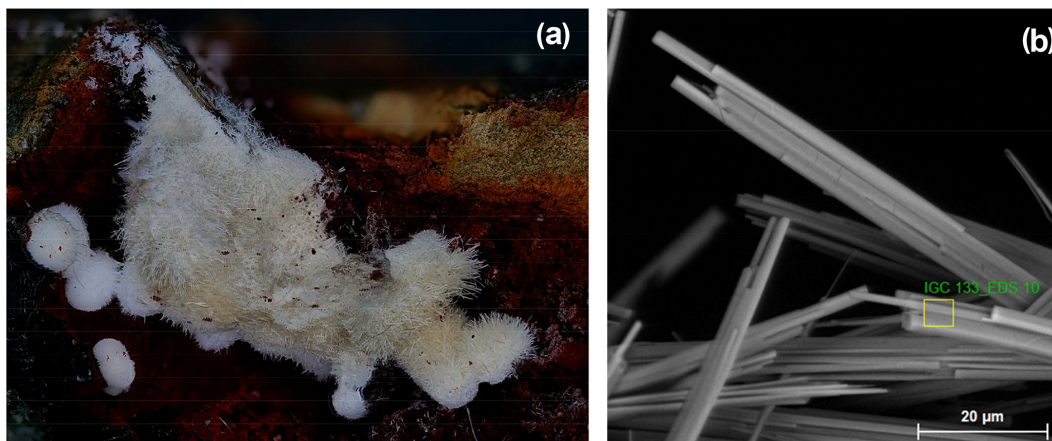


**Figure 2.** (a) Clusters of white needles of allanpringite/strunzite in specimen IGC133 (FOV = 4.9 mm). (b) Characteristic form of crystals, showing central strunzite needle with epitaxial allanpringite needles on either side.

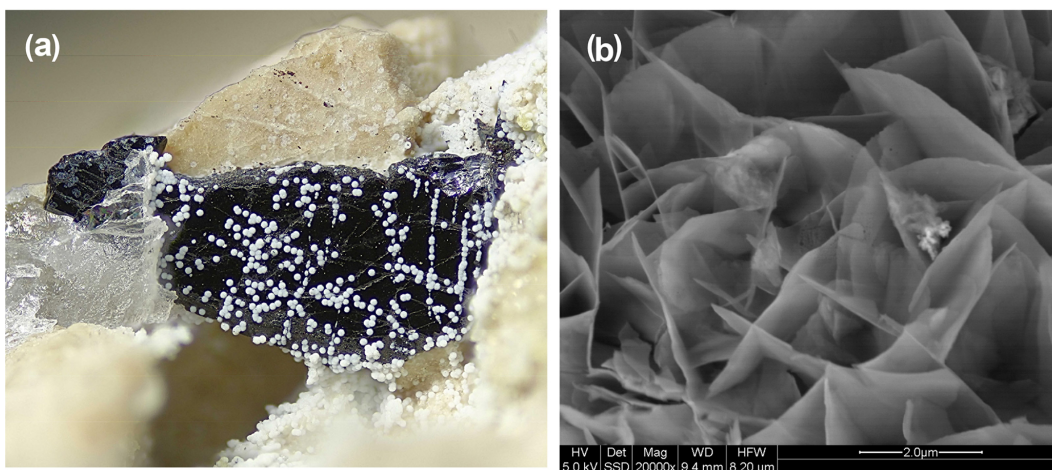


**Figure 3.** (a) White spheroids of iangreyite on black columbite and yellow altered zwieselite (FOV = 2.4 mm). Photo by Volker Betz. (b) SEM BSE image of microtexture of an iangreyite spheroid.

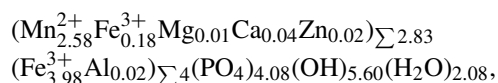
studied here all belong to his “Paragenesis Table II – Rock-bridgeite and zwieselite-bearing subparageneses”. Kennngottite and nizamoffite fit in his scheme II-C, allanpringite in scheme II-D and iangreyite in scheme II-B.

## 4 Results and discussion

### 4.1 Kennngottite

EMP analyses for kennngottite laths from specimen Hag510 (Fig. 1c) are reported in Table 1.

The empirical formula, based on 24 anions, is



which compares with the ideal formula

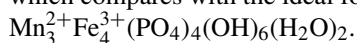


**Table 1.** EMP analyses with standard deviations in brackets.

	Kennngottite Hag510, $n = 9$	Strunzite IGC133, $n = 3$	Allanpringite IGC133, $n = 2$
MnO	20.6 (1.1)	11.7 (0.4)	3.67 (1.98)
MgO	0.03 (0.07)	0.76 (0.24)	0.86 (0.45)
ZnO	0.21 (0.12)	0.36 (0.08)	0.39 (0.09)
CaO	0.25 (0.08)	n.d. <sup>b</sup>	0.11 (0.03)
Al <sub>2</sub> O <sub>3</sub>	0.13 (0.09)	2.72 (1.17)	0.80 (0.07)
Fe <sub>2</sub> O <sub>3</sub>	37.4 (1.1)	28.6 (2.2)	40.7 (2.3)
P <sub>2</sub> O <sub>5</sub>	32.6 (1.3)	28.4 (0.7)	26.7 (0.4)
H <sub>2</sub> O <sup>a</sup>	9.9	26.6	23.5
Total	101.1	99.1	96.6

<sup>a</sup> H<sub>2</sub>O from ideal structural formulae; <sup>b</sup> n.d.: not detected.



**Figure 4.** Colourless 2 mm wide crystal mass of transparent nizamoffite from Hagendorf Süd, associated with black Mn oxides and yellow laueite crystals. Photo by Christian Rewitzer.

EMP analyses were also obtained for the earthy form of kenngottite, but the sub-micrometre thickness of the crystals (Fig. 1b) resulted in very low analysis totals.

The phase purity of the yellow laths in specimen Hag510 was checked by obtaining a Gandolfi pattern. The pattern could be completely indexed using the kenngottite crystal structure, with no impurity peaks.

Single-crystal diffracting quality of individual laths was checked at the Australian Synchrotron MX2 microfocus beamline. The diffraction patterns showed split spots due to the laths being composed of sub-parallel fibres. A lath giving the cleanest pattern was used for a data collection and structure refinement. A SHELXT structure solution (Sheldrick, 2015) gave a model in space group  $P2_1/a$  that matched the published structure for kenngottite, including a disordering of Fe atoms and a coordinated anion over pairs of sites Fe2a/Fe2b, Fe3a/Fe3b and O12a/O12b (Sejkora et al., 2019). Anisotropic refinement for all atoms except the low-occupation, disordered sites converged to  $wR_{\text{obs}} = 0.053$  for 1812 independent reflections. Further details of the data collection and refinement are summarised in Table 2. Refined coordinates, equivalent isotropic displacement parameters and bond-valence sums (BVSs) based on the parameters of Gagné and Hawthorne (2015) are reported in Table 3, and polyhedral bond distances are given in Table 4.

The mean octahedral bond lengths and associated BVS values are consistent with predominantly  $\text{Mn}^{2+}$  in the Mn1 and Mn2 sites and  $\text{Fe}^{3+}$  in the Fe1, Fe2 and Fe3 sites. The BVS values are close to 1 for the sites O9 to O12, representing eight anions pfu (per formula unit). For the ideal formula, only six  $\text{OH}^-$  are required for charge balance, so the sum of the anions at sites O9 to O12 corresponds to six  $\text{OH}^- + 2\text{H}_2\text{O}$ , where the  $\text{H}_2\text{O}$  is most likely disordered over all four sites. A similar disordering of  $\text{OH}^-$  and  $\text{H}_2\text{O}$  was

reported for the crystal structure of the type kenngottite (Sejkora et al., 2019).

The only published crystal structure of kenngottite for comparison is by Sejkora et al. (2019). They noted the poor diffracting quality of the fibrous crystals, which restricted the reflection data used in their laboratory SC refinement to a resolution of 1.2 Å. The synchrotron-based SC dataset reported here has more than 3 times the number of independent reflections, and the refined bond distances have associated standard deviations up to an order of magnitude smaller. Despite the improved quality of the refinement, the derived structural parameters are generally not significantly different from those of Sejkora et al. (2019).

It is interesting to note that the structure refinement for kenngottite from the Hagendorf Süd pegmatite gave the same extent of disordering of the Fe2a/Fe2b and Fe3a/Fe3b sites (0.73/0.27) as for the specimen from Krásno (0.75(2)/0.25(2)), within the SDs of the latter study. A possible explanation can be given in terms of fine-scale mixing of domains of kenngottite and souzalite structures. Souzalite has the same structural formula as kenngottite, written generally as  $\text{M1}^{2+}(\text{M2}^{2+})_2\text{M1}^{3+}(\text{M3}^{3+})_2(\text{PO}_4)_4(\text{OH})_6 \cdot 2\text{H}_2\text{O}$ , where  $\text{M}^{2+}$  is Mg and  $\text{M}^{3+}$  is Al for souzalite. It has triclinic symmetry, with  $a = 7.222 \text{ \AA}$ ,  $b = 11.780 \text{ \AA}$ ,  $c = 5.117 \text{ \AA}$ ,  $\alpha = 90.16^\circ$ ,  $\beta = 109.94^\circ$  and  $\gamma = 81.33^\circ$  (Le Bail et al., 2003). The kenngottite cell parameters are related to the souzalite cell parameters by the transformation (2 1 0, 0 0 -1, 0 -1 0). Both structures contain face-shared octahedral trimers  $\text{M2}^{2+}\text{-M1}^{3+}\text{-M2}^{2+}$ , connected via edge sharing with  $\text{M1}^{2+}$ -centred octahedra to form chains along  $[001]_{\text{kenn}} \equiv [010]_{\text{souz}}$  that corner-connect with  $\text{PO}_4$  tetrahedra into (100) layers. These layers alternate with (100) layers containing corner-connected octahedral trimers  $\text{M3}^{3+}\text{-M2}^{3+}\text{-M3}^{3+}$  as shown in Fig. 5 for kenngottite. The main difference between the structures of the two minerals concerns the relative locations along the 5 Å axis of the corner-connected octahedral trimers in successive (100) planes. This is illustrated in Fig. 6. In kenngottite, the trimers in successive (100) planes are all at the same level along the 5 Å axis, whereas in souzalite, the trimers in successive (100) planes are displaced by half of the 5 Å axis. Thus in kenngottite the  $\text{M3}^{3+}\text{-M2}^{3+}\text{-M3}^{3+}$  trimers lie in  $(010)_{\text{kenn}}$  planes, whereas in souzalite they lie in  $(110)_{\text{kenn}}$  planes. In souzalite, half of the trimers occupy sites that are vacant in the ideal kenngottite structure. In the actual kenngottite structure, these sites are 25 % occupied, whereas the sites that are fully occupied in the ideal structure are 75 % occupied. This distribution can be attributed to a fine-scale equal-volume 1 : 1 mixing of domains of the souzalite-type and kenngottite-type structures. Such intergrowths would occur parallel to (100) planes. Le Bail et al. (2003) noted that souzalite displays polysynthetic twinning on (100) planes. The twinning produces local regions of a kenngottite-type structure at the twin boundary.

**Table 2.** Crystal data and structure refinement for kenngottite.

Ideal formula	$\text{Mn}_3^{2+}\text{Fe}_4^{3+}(\text{PO}_4)_4(\text{OH})_6(\text{H}_2\text{O})_2$
Formula weight	906.1
Temperature	100 K
Wavelength	0.71073 Å
Space group	$P2/a$
Unit-cell dimensions	$a = 13.983(3)$ Å $b = 5.2070(10)$ Å $c = 12.200(2)$ Å $\beta = 98.84(3)^\circ$
Volume	877.7(3) Å <sup>3</sup>
Z	2
Absorption correction	Multiscan, $\mu = 5.80 \text{ mm}^{-1}$
Crystal size	0.02 × 0.04 × 0.11 mm <sup>3</sup>
Theta range for data collection	1.69 to 31.98°.
Index ranges	$-18 \leq h \leq 18, -7 \leq k \leq 7, -17 \leq l \leq 17$
Reflections collected	14 307
Independent reflections	1812
Reflections with $I_o > 3\sigma(I)$	1269
Refinement method	Full-matrix least squares on $F$
Data/restraints/parameters	1812/0/168
Final $R$ indices [ $I > 3\sigma(I)$ ]	$R_{\text{obs}} = 0.042, wR_{\text{obs}} = 0.049$
$R$ indices (all data)	$R_{\text{obs}} = 0.061, wR_{\text{obs}} = 0.053$
Largest diff. peak and hole	1.14 and $-0.67 \text{ e Å}^{-3}$

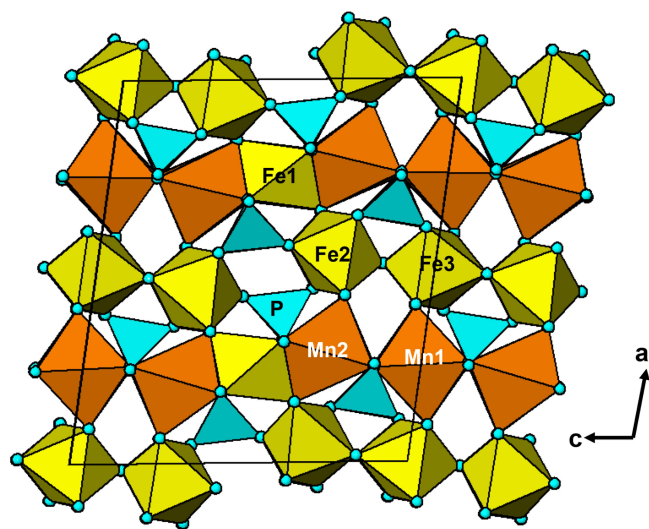
**Table 3.** Atom coordinates, equivalent isotropic displacement parameters (Å<sup>2</sup>) and bond-valence sums (BVSs) for kenngottite.

	$x$	$y$	$z$	$U_{\text{eq}}$	BVS
Fe1	0.25	0.24048(11)	0.5	0.0210(2)	3.08
Fe2a	0.5	0.5	0	0.0165(2)	3.14
Fe2b	0.5	1	0	0.0215(7)	3.54
Fe3a	0.54749(5)	0.48602(11)	0.30695(5)	0.01628(16)	2.94
Fe3b	0.45189(15)	0.9888(4)	0.69275(16)	0.0196(6)	2.83
Mn1	0.25	0.25800(11)	1	0.0205(2)	2.17
Mn2	0.21337(5)	0.25159(8)	0.72710(5)	0.0228(2)	2.10
P1	0.31335(8)	0.74872(13)	0.85663(8)	0.0195(3)	5.00
P2	0.38185(7)	0.73891(13)	0.43929(8)	0.0188(3)	4.89
O1	0.3916(2)	0.7453(3)	0.9601(3)	0.0215(8)	1.77
O2	0.3564(2)	0.7443(3)	0.7500(2)	0.0191(7)	1.80
O3	0.25483(18)	0.9988(5)	0.86143(19)	0.0210(6)	1.99
O4	0.24956(19)	0.5090(5)	0.8617(2)	0.0237(7)	2.02
O5	0.4358(2)	0.7316(4)	0.5589(2)	0.0254(8)	1.75
O6	0.31987(19)	0.9877(5)	0.42060(18)	0.0218(7)	2.03
O7	0.4506(2)	0.7403(4)	0.3531(2)	0.0229(8)	1.71
O8	0.31712(18)	0.4958(4)	0.41874(18)	0.0207(6)	2.10
O9	0.3481(2)	0.2456(4)	0.6452(3)	0.0237(8)	1.18
O10	0.4371(2)	0.2305(4)	0.2526(2)	0.0242(8)	0.82
O11	0.5925(3)	0.7668(4)	$-0.0419(3)$	0.0273(9)	0.89
O12a	0.5094(3)	0.6378(7)	0.1540(3)	0.0250(8)	1.05
O12b	0.5060(10)	0.866(2)	0.1509(12)	0.037(3)	1.49

Site occupancies: Fe2a/Fe2b = 0.732(2)/0.268, Fe3a/Fe3b = 0.728(2)/0.237, O12a/O12b = 0.756(6)/0.244.

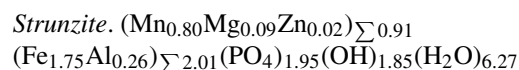
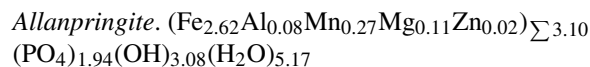
**Table 4.** Polyhedral bond lengths (Å) for kenngottite.

Fe1-O6 x2	1.979(3)		
Fe1-O8 x2	1.979(2)		
Fe1-O9 x2	2.067(3)		
Avg	2.008		
Fe2a-O1 x2	1.985(2)	Fe2b-O1 x2	2.017(2)
Fe2a-O11 x2	2.017(3)	Fe2b-O11 x2	1.901(3)
Fe2a-O12a x2	1.997(4)	Fe2b-O12b x2	1.959(14)
Avg	2.000	Avg	1.959
Fe3a-O2	2.003(3)	Fe3b-O2	2.044(3)
Fe3a-O5	1.975(3)	Fe3b-O5	2.097(3)
Fe3a-O7	2.035(3)	Fe3b-O7	2.097(3)
Fe3a-O9	2.041(3)	Fe3b-O9	1.993(3)
Fe3a-O10	2.068(3)	Fe3b-O10	1.959(3)
Fe3a-O12a	2.021(4)	Fe3b-O12b	2.053(14)
Avg	2.024	Avg	2.040
Mn1-O3 x2	2.172(2)	Mn2-O3	2.113(2)
Mn1-O4 x2	2.134(3)	Mn2-O4	2.120(2)
Mn1-O11 x2	2.187(3)	Mn2-O6	2.257(2)
Avg	2.164	Mn2-O8	2.175(2)
		Mn2-O9	2.264(3)
		Mn2-O10	2.159(3)
		Avg	2.181
P1-O1	1.539(3)	P2-O5	1.537(3)
P1-O2	1.516(3)	P2-O6	1.556(3)
P1-O3	1.544(3)	P2-O7	1.530(3)
P1-O4	1.541(3)	P2-O8	1.554(2)
Avg	1.535	Avg	1.544

**Figure 5.** A [010] projection of the crystal structure of kenngottite, showing trimers of face-shared octahedra Mn2-Fe1-Mn2, connected into chains via edge sharing with Mn2-centred octahedra, and trimers of corner-connected octahedra Fe2-Fe3-Fe2 connected into chains via PO<sub>4</sub> tetrahedra.

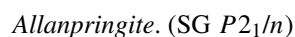
## 4.2 Allanpringite

EMP analyses of allanpringite and associated Al-bearing strunzite are given in Table 1. The empirical formulae, based on 16 anions, are the following.

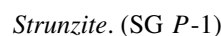


The empirical formulae compare with the ideal end-member compositions,  $\text{Fe}_3^{3+}(\text{PO}_4)_2(\text{OH})_3 \cdot 5\text{H}_2\text{O}$  and  $\text{Mn}^{2+}\text{Fe}_2^{3+}(\text{PO}_4)_2(\text{OH})_2 \cdot 6\text{H}_2\text{O}$ , respectively. Allanpringite contains significant levels of Mn, Mg and Zn, which are not present in the type mineral (Kolitsch et al., 2006). The epitaxially grown pairs of minerals that were analysed had widths of only  $\sim 2\ \mu\text{m}$ , so the extra elements in the allanpringite analyses may be due to contributions from the adjacent strunzite. Alternatively, the extra cations may be located in the large eight-sided channels along [010] (Fig. 7).

Attempts to obtain synchrotron SC data on the allanpringite were thwarted by the composite nature of the crystals (Fig. 2b). Instead, a PXRD dataset was refined by the Rietveld method using a two-phase model incorporating published SC coordinates for strunzite and allanpringite (Grey and Kampf, 2018; Kolitsch et al., 2006). Profile and unit-cell parameters were refined to  $R_{\text{wp}} = 2.61$  and  $\Psi^2 = 7.5$ . The fit to the experimental profile is shown in Fig. 8. The Rietveld-based quantitative phase analysis gave 45 wt % allanpringite plus 55 wt % strunzite. The refined unit-cell parameters for the two phases are the following.



$$a = 9.757(2)\ \text{\AA}, b = 7.341(1)\ \text{\AA}, c = 17.808(4)\ \text{\AA}, \\ \beta = 92.20(2)^\circ$$



$$a = 10.270(2)\ \text{\AA}, b = 9.829(2)\ \text{\AA}, c = 7.289(1)\ \text{\AA}, \\ \alpha = 91.01(2)^\circ, \beta = 98.66(2)^\circ, \gamma = 117.34(1)^\circ$$

The close match of the  $a$  and  $b$  parameters for allanpringite to the  $b$  and  $c$  parameters for strunzite is the basis for the epitaxial growth of allanpringite on strunzite. The pairs of unit-cell parameters differ by only 0.7%. The (001) planes in allanpringite and (100) planes in strunzite contain identical structural motifs, comprising 7.3 Å chains of corner-connected octahedra that are interconnected along the 9.8 Å axis by corner linking to PO<sub>4</sub> tetrahedra, as illustrated in Fig. 9. Relief of the strain associated with the small mismatch between the unit-cell parameters of the two structures may be the cause of the transverse cracks in the central strunzite needle shown in Fig. 2b.

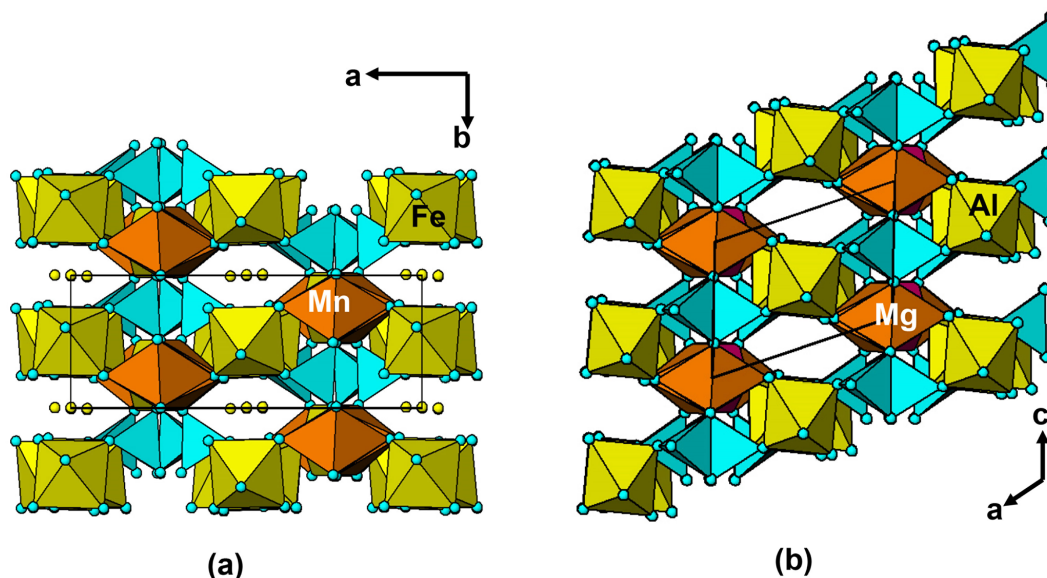


**Figure 6.** Common projections of the crystal structures of (a) kenngottite and (b) souzalite, showing the different relative locations of the corner-connected octahedral trimers (yellow octahedra) in successive (100) planes in the two structures.

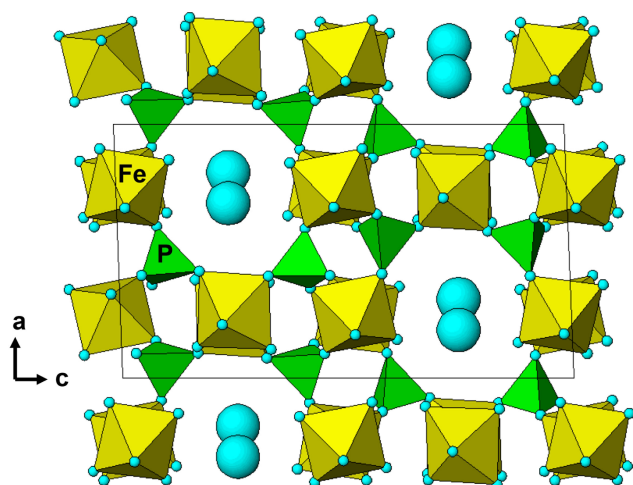


**Figure 7.** A [010] projection of the crystal structure of allanpringite, showing eight-sided channels occupied by water molecules (blue spheres). The channels are potential locations for extra-framework hydrated cations.

### 4.3 Iangreyite

The microtexture of the spheroids of iangreyite crystals, comprising curved, ultrathin laths, was not conducive to getting quantitative EMP analyses. Semiquantitative analyses were obtained by EDS and are reported in Table 5. The  $\text{Al}_2\text{O}_3$  and  $\text{P}_2\text{O}_5$  analyses are in good agreement with published analyses for the Krásno mineral (Mills et al., 2011), but the CaO is 50% higher. In the published refinement of the iangreyite structure, the Ca2 site is only

**Table 5.** EDS analyses with standard deviations in brackets.

	Iangreyite	Nizamoffite
	IGC112, $n = 4$	REM 3600, $n = 4$
$\text{P}_2\text{O}_5$	27.7 (1.4)	24.7 (2.2)
ZnO	34.0 (2.2)	n.d.
MnO	12.8 (0.9)	n.d.
CaO	n.d.*	16.9 (1.7)
$\text{Al}_2\text{O}_3$	n.d.	28.5 (3.0)
$\text{SiO}_2$	n.d.	4.55 (1.47)
F	n.d.	5.00 (0.65)

\* n.d.: not detected.

half occupied. Full occupation of this site in the Hagen-dorf Süd mineral may explain the difference. We confirmed the higher occupation of the Ca2 site in the Hagen-dorf Süd mineral by Rietveld refinement. The EDS analyses confirm that a high F content is characteristic of iangreyite, although the value is lower than in the two co-type specimens (8 wt%–9 wt%). The Hagen-dorf mineral contains twice the amount of  $\text{SiO}_2$  compared to the Krásno type mineral, due to fine-scale association of iangreyite with perhamite,  $\text{Ca}_3\text{Al}_7(\text{SiO}_4)_3(\text{PO}_4)_4(\text{OH})_3 \cdot 16.5\text{H}_2\text{O}$ , as confirmed by PXRD.

Rietveld profile refinement was conducted on PXRD data collected on ground spheroids in specimen IGC112. The sparse amount of material, presence of impurities and asymmetric peak broadening of the (001) reflections (Fig. 10) restricted the quality of the refinement ( $R_{\text{wp}} = 8.4$ ,  $\Psi^2 = 4.0$ ). The main impurity phase was perhamite. A two-phase Ri-

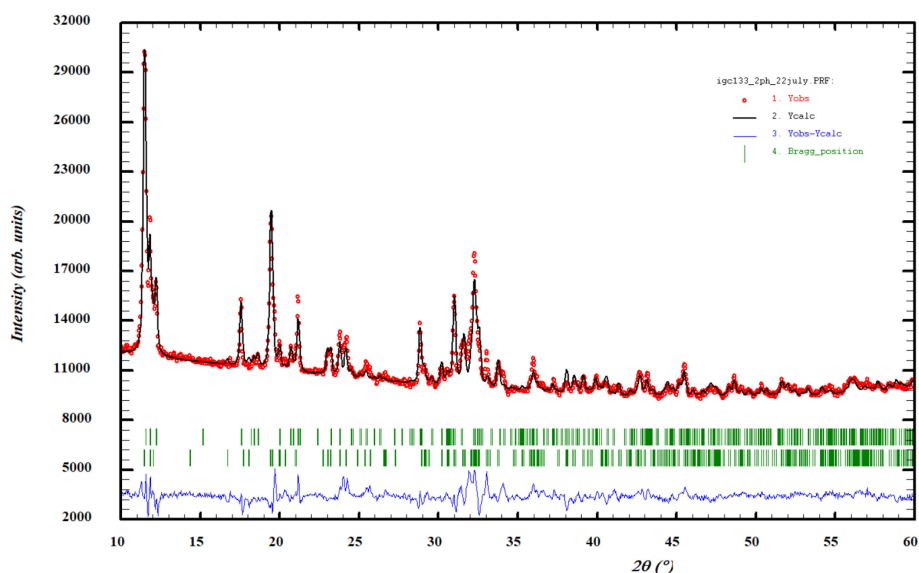


**Figure 8.** Rietveld profile fitting to a PXRD pattern for specimen IGC133, with a two-phase mixture of allanpringite and strunzite. Red dots represent experimental values, and the black line represents the fitted pattern. Green markers are Bragg reflections for allanpringite (upper) and strunzite (lower). Blue line is the difference plot.

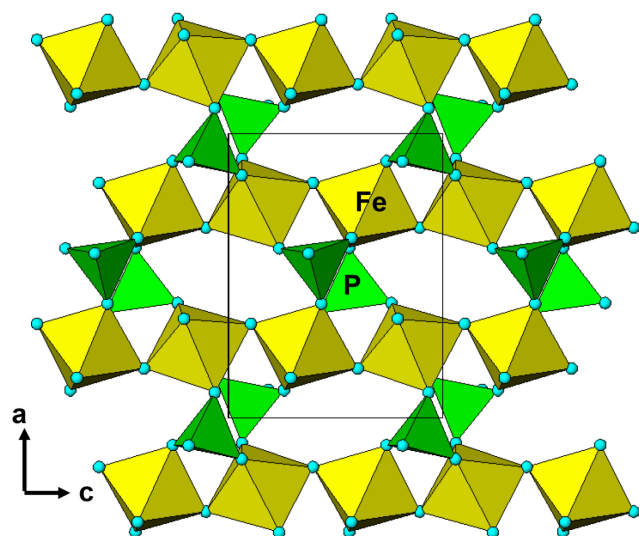


**Figure 9.** A (010) slice of the allanpringite crystal structure, equivalent to a (100) slice of the strunzite crystal structure, having the same corner-connected chains of Fe-centred octahedra interconnected via corner sharing with  $\text{PO}_4$  tetrahedra.

etveld refinement gave a quantitative XRD (X-ray diffraction) phase analysis result of 60 wt % iangreyite and 40 wt % perhamite. The presence of perhamite in the spheroids would help explain the elevated silica content and the lower F content from the EDS analyses. Refined unit-cell parameters from the Rietveld refinement are the following.

*Iangreyite.* (SG *P321*)

$$a = 7.008(2) \text{ \AA}, c = 16.952(2) \text{ \AA}$$

*Perhamite.* (SG *P321*)

$$a = 6.998(1) \text{ \AA}, c = 20.177(8) \text{ \AA}$$

The unit-cell parameters for iangreyite are higher than those for the two co-types, particularly the  $c$  parameter, which is 1.0% higher than for the Krásno mineral ( $c = 16.782 \text{ \AA}$ ). A plot of the low-angle part of the fitted diffraction pattern for the Hagendorf Süd two-phase mixture of iangreyite and perhamite (Fig. 10) shows a broadened asymmetric peak for  $(001)_{\text{iang}}$ , with asymmetry on the low-angle side, towards the  $(001)_{\text{perh}}$  peak for perhamite. Mills et al. (2011) commented that iangreyite appeared to be a low-temperature alteration product of perhamite, where Si and some Al are leached from the layer structure, causing a shrinking along  $[001]$ . The pattern shown in Fig. 10 confirms this with the asymmetry of  $(001)_{\text{iang}}$  suggestive of a range of compositions intermediate between those of perhamite and iangreyite. The relationship between the two structures is shown in Fig. 11. The  $\text{Si}_3\text{O}_9$  rings in perhamite are leached, and the pairs of  $\text{AlO}_4$  tetrahedra on either side of the  $\text{Si}_3\text{O}_9$  rings are replaced by  $\text{AlO}_2(\text{OH})_3$  trigonal bipyramids in the formation of iangreyite.

#### 4.4 Nizamoffite

Nizamoffite was characterised using EDS analyses and PXRD. The EDS analyses are reported in Table 5. The atom ratios, when scaled to eight anions and with  $\text{H}_2\text{O}$  added to be consistent with the structure, give the formula  $\text{Mn}_{0.9}\text{Zn}_{2.1}(\text{PO}_4)_2(\text{H}_2\text{O})_4$ , corresponding to a solid solution of 10% hopeite,  $\text{Zn}_3(\text{PO}_4)_2(\text{H}_2\text{O})_4$ , in nizamoffite. Rietveld

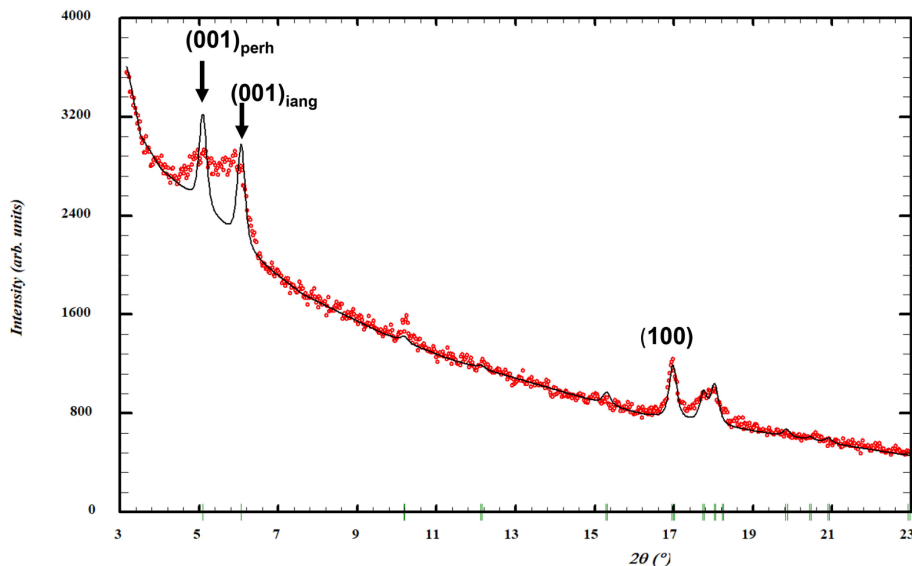


**Figure 10.** Low-angle region of a PXRD pattern for specimen IGC112. Red dots represent experimental values, and the black line represents a Rietveld-fitted profile with a two-phase mixture of iangreyite plus perhamite. The refined peak width matches the experimental width for the (100) reflection but is too narrow for the (001) reflections.

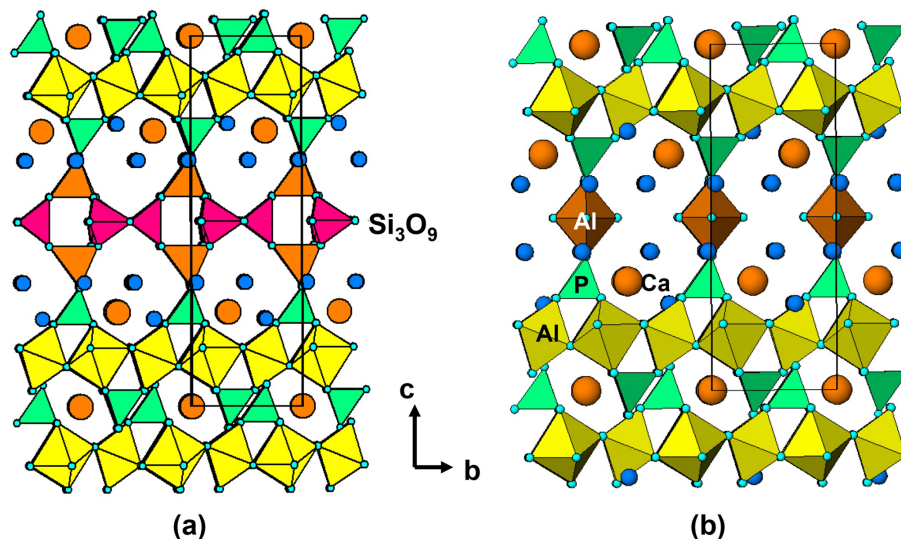


**Figure 11.** Two [100] projections of the crystal structures of (a) perhamite and (b) iangreyite, showing the absence of  $\text{Si}_3\text{O}_9$  groups and the replacement of  $\text{AlO}_4$  tetrahedra (orange) by Al-centred trigonal prisms (brown) in iangreyite.

refinement of the PXRD data gave the unit-cell parameters  $a = 10.653(1) \text{ \AA}$ ,  $b = 18.498(1) \text{ \AA}$  and  $c = 5.0577(4) \text{ \AA}$ .

Nizamoffite is isostructural with hopeite, containing kinked chains of  $\text{ZnO}_4$  tetrahedra along [001] that are interconnected via corner sharing with  $\text{PO}_4$  tetrahedra to form (010) sheets (Kampf et al., 2013). The sheets are linked along [010] via  $\text{MnO}_2(\text{H}_2\text{O})_4$  octahedra, which share corners with the  $\text{PO}_4$  tetrahedra (Fig. 12a). The (010) sheets of composition  $[\text{Zn}(\text{PO}_4)]_2$  in nizamoffite are chemically and topologically identical to the (100) sheets

in the Hagendorf Süd type-locality mineral steinmetzite,  $\text{Fe}^{3+}[\text{Zn}(\text{PO}_4)]_2(\text{OH})(\text{H}_2\text{O})_3$  (Grey et al., 2017), and phosphophyllite,  $\text{Fe}^{2+}[\text{Zn}(\text{PO}_4)]_2(\text{H}_2\text{O})_4$  (Hill, 1977). The structures for nizamoffite and steinmetzite differ in the way the sheets are linked. In nizamoffite, the O atoms of the linking octahedra are in a *cis* configuration, whereas in steinmetzite (and phosphophyllite), the O atoms of the linking octahedra are in a *trans* configuration (Fig. 12b). It is interesting that nizamoffite at Hagendorf Süd is related to the alteration of rockbridegite and belongs in Mücke's (1981) rockbridegite

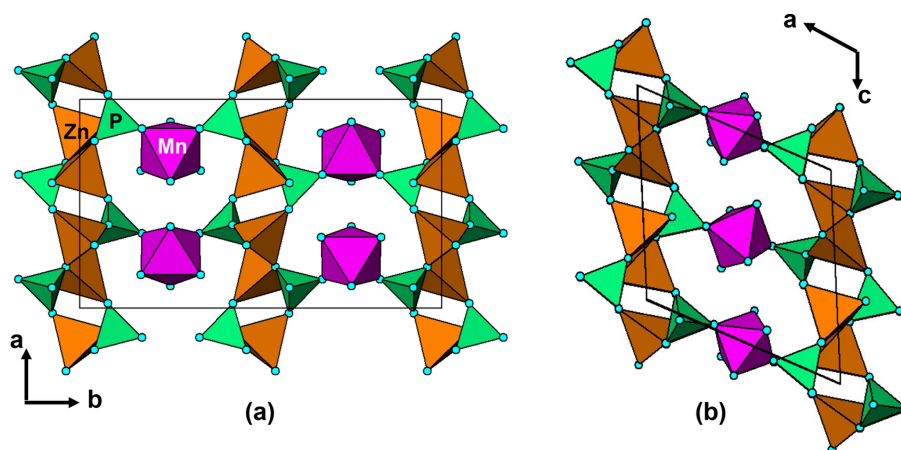


**Figure 12.** (a) A [001] projection of the structure of nizamoffite compared to (b) a [010] projection of the structure of steinmetzite, showing the (010) layers of corner-connected tetrahedra of composition  $[\text{Zn}(\text{PO}_4)_2]$  that are common to both structures and the different types of linkage of the layers with corner-connected octahedra (purple).

paragenesis scheme II-C, whereas steinmetzite forms from the alteration (oxidation) of phosphophyllite, which fits with Mücke's (1981) rockbridgeite-free paragenesis scheme I-C.

## 5 Concluding remarks

Although the Hagendorf Süd pegmatite mine has been closed for almost 40 years, new type-locality secondary phosphate minerals continue to be identified in specimens from the mine that are now in extensive museum and private collections. This year, two potentially new type-locality minerals have been characterised and mineral naming proposals have been submitted to the IMA (International Mineralogical Association) CNMNC. They are a new member of the whiteite group and a species related to benyacarite. In the course of characterising the first occurrences of secondary phosphate minerals described here, another potentially new secondary phosphate species, part of the rockbridgeite group, has been identified. Work is in progress on its characterisation.

**Data availability.** Crystallographic data for kenngottite are available in the Supplement.

**Supplement.** The supplement related to this article is available online at: <https://doi.org/10.5194/ejm-34-439-2022-supplement>.

**Author contributions.** EK initiated the study and provided specimens and specimen descriptions. RH and CR provided specimens, sample descriptions, specimen photos and EDS/PXRD data for nizamoffite. IEG coordinated the research, analysed the data and wrote the paper. CMM conducted the EMP analyses. SB collected and processed the synchrotron (SR) SC data. WGM helped anal-

yse the data. AMG conducted ESEM studies. CD prepared polished mounts for EMP analyses.

**Competing interests.** The contact author has declared that none of the authors has any competing interests.

**Disclaimer.** Publisher's note: Copernicus Publications remains neutral with regard to jurisdictional claims in published maps and institutional affiliations.

**Acknowledgements.** Thanks to Volker Betz for the colour photographs of kenngottite, allanpringite and iangreyite. We thank Anthony Kampf for obtaining a Gandolfi PXRD pattern on kenngottite crystals in specimen Hag510. This research was undertaken in part using the MX2 beamline at the Australian Synchrotron, part of ANSTO (Australian Nuclear Science and Technology Organisation), and made use of the Australian Cancer Research Foundation detector. We acknowledge the Diffraction Laboratory at CSIRO Mineral Resources, Clayton, for use of their Philips X'PERT MPD powder XRD diffractometer.

**Review statement.** This paper was edited by Sergey Krivovichev and reviewed by Anthony Kampf and one anonymous referee.

## References

- Aragao, D., Aishima, J., Cherukuvada, H., Clarken, R., Clift, M., Cowieson, N. P., Ericsson, D. J., Gee, C. L., Macedo, S., Mudie, N., Panjekar, S., Price, J. R., Riboldi-Tunnicliffe, A., Rostan, R., Williamson, R., and Caradoc-Davies, T. T.: MX2: a high-flux undulator microfocus beamline serving both the chemical and

- macromolecular crystallography communities at the Australian Synchrotron, *J. Synch. Radiat.*, 25, 885–891, 2018.
- Birch, W. D., Grey, I. E., Keck, E., Mills, S. M., and Mumme, W. G.: The Hagendorf Süd pegmatite: Australian-Bavarian collaboration on the characterization of new secondary phosphate minerals, *Aust. J. Mineral.*, 19, 7–19, 2018.
- Dill, H. G.: The Hagendorf-Pleystein province: the centre of pegmatites in an ensialic orogeny, Springer, Hanover, Germany, ISBN 978-3-319-18805-8, 2015.
- Farrugia, L. J.: WinGX suite for small molecule single-crystal crystallography, *J. Appl. Crystallogr.*, 32, 837–838, 1999.
- Forster, A. and Kummer, R.: The pegmatites in the area of Pleystein-Hagendorf/North Eastern Bavaria, *Fortsch. Mineral.*, 52, 89–99, 1974.
- Gagné, O. C. and Hawthorne, F. C.: Comprehensive derivation of bond-valence parameters for ion pairs involving oxygen, *Acta Crystallogr. B*, 71, 562–578, 2015.
- Grey, I. E. and Kampf, A. R.: Zeolitic water in strunzite-group minerals, *Mineral. Mag.*, 82, 291–299, 2018.
- Grey, I. E., Keck, E., Kampf, A. R., Mumme, W. G., MacRae, C. M., Gable, R. W., Glenn, A. M., and Davidson, C. J.: Steinmetzite,  $Zn_2Fe^{3+}(PO_4)_2(OH) \cdot 3H_2O$ , a new mineral formed from alteration of phosphophyllite at the Hagendorf Süd pegmatite, Bavaria: *Mineral. Mag.*, 81, 329–338, 2017.
- Grey, I. E., Kampf, A. R., Keck, E., Cashion, J. D., MacRae, C. M., Gozukara, Y., Peterson, V. K., and Shanks, F. L.: The rock-bridgeite group approved and a new member, ferrockbridgeite,  $(Fe^{2+}, Mn^{2+})_2(Fe^{3+})_3(PO_4)_3(OH)_4(H_2O)$ , described from the Hagendorf Süd pegmatite, Oberpfalz, Bavaria, *Eur. J. Mineral.*, 31, 389–397, <https://doi.org/10.1127/ejm/2019/0031-2823>, 2019.
- Hill, R. J.: The crystal structure of phosphophyllite, *Am. Mineral.*, 62, 812–817, 1977.
- Kampf, A. R., Falster, A. U., Simmons, W. B., and Whitmore, R. W.: Nizamoffite,  $Mn^{2+}Zn_2(PO_4)_2(H_2O)_4$ , the Mn analogue of hopeite from the Palermo No. 1 pegmatite, North Groton, New Hampshire, *Am. Mineral.*, 98, 1893–1898, 2013.
- Keck, E.: Phosphatminerale und deren Auftreten in verschiedenen Teufen im Pegmatit von Hagendorf-Süd, *Aufschluss*, 34, 307–316, 1983.
- Kolitsch, U., Bernhardt, H.-J., Lengauer, C.L., Blass, G. and Tillmans, E.: Allanpringite,  $Fe_3^{3+}(PO_4)_2(OH)_3 \cdot 5H_2O$ , a new ferric iron phosphate from Germany, and its close relationship to wavellite, *Eur. J. Mineral.*, 18, 793–801, <https://doi.org/10.1127/0935-1221/2006/0018-0793>, 2006.
- Le Bail, A., Stephens, P. W., and Hubert, F.: A crystal structure for the souzalite/gormanite series from synchrotron powder diffraction data, *Eur. J. Mineral.*, 15, 719–723, <https://doi.org/10.1127/0935-1221/2003/0015-0719>, 2003.
- Mills, S., Mumme, G., Grey, I., and Bordet, P.: The crystal structure of perhamite, *Mineral. Mag.*, 70, 201–209, 2006.
- Mills, S. J., Kampf, A. R., Sejkora, J., Adams, P. M., Birch, W. D., and Plasil, J.: Iangreyite: a new secondary phosphate mineral closely related to perhamite, *Mineral. Mag.*, 75, 327–336, 2011.
- Mücke, A.: The paragenesis of the phosphate minerals of the Hagendorf pegmatite – a general view, *Chem. Erde-Geochem.*, 40, 217–234, 1981.
- Mücke, A., Keck, E., and Rose, D.: Hagendorf-Süd, *Lapis*, 6, 9–26, 1981.
- Petříček, V., Dušek, M., and Palatinus, L.: Crystallographic Computing System JANA2006: General features, *Z. Kristallogr.*, 229, 345–352, 2014.
- Rodriguez-Carvajal, J.: FULLPROF: A Program for Rietveld refinement and Pattern Matching Analysis: Satellite meeting on powder diffraction of the Fifteenth General Assembly and International Congress of Crystallography, 16–19 July 1990, Toulouse, France, 1990.
- Schmid, H.: Verbandsverhältnisse der Pegmatite des Oberpfälzer und des Bayerischen Waldes (Hagendorf-Pleystein-Hühnerkobel), *Neues Jahrb. Mineral. Abh.*, 88, 309–404, 1955.
- Sejkora, J., Grey, I. E., and Kampf, A. R.: Kenngottite,  $Mn_3^{2+}Fe_4^{3+}(PO_4)_4(OH)_6(H_2O)_2$ : a new phosphate mineral from Krásno near Horní Slavkov, Czech Republic, *Eur. J. Mineral.*, 31, 629–636, <https://doi.org/10.1127/ejm/2019/0031-2855>, 2019.
- Sheldrick, G. M.: Crystal-structure refinement with SHELX, *Acta Crystallogr. C*, 71, 3–8, 2015.
- Strunz, H., Forster, A., and Tennyson, C.: Die Pegmatite der nördlichen Oberpfalz, *Aufschluss*, 26, 117–189, 1975.
- Vrtiska, L., Sejkora, J. and Malikova, R.: A study of secondary phosphates with allanpringite and tvrdyite from the abandoned iron deposit Krusna hora near Beroun (Czech Republic), *Bull. Mineral. Petrol.*, 27, 231–246, 2019.
- Vrtiska, L., Zemek, V., and Malikova, R.: Rare allanpringite-alteration product of wavellite from Milina quarry near Zajecov (Czech Republic), *Bull. Mineral. Petrol.* 28, 126–131, 2020.